JB Journals.ASM.org

Functional and Structural Study of the Dimeric Inner Membrane Protein SbmA

Natalia Corbalan,[a] Giulia Runti,[b] Conrado Adler,[a] Sonia Covaceuszach,[c] Robert C. Ford,[d] Doriano Lamba,[c] Konstantinos Beis,[e,f,g] Marco Scocchi,[b] Paula A. Vincent[a]

Instituto Superior de Investigaciones Biológica, INSIBIO (Consejo Nacional de Investigaciones Científicas y Técnicas-Universidad Nacional de Tucumán), San Miguel de Tucumán, Tucumán, Argentina[a]; Department of Life Sciences, University of Trieste, Trieste, Italy[b]; Istituto di Cristallografia, Consiglio Nazionale delle Ricerche, U.O.S di Trieste, Area Science Park—Basovizza, Trieste, Italy[c]; Faculty of Life Sciences, University of Manchester, Manchester Interdisciplinary Biocentre, Manchester, United Kingdom[d]; Division of Molecular Biosciences, Imperial College London, South Kensington, London, United Kingdom[e]; Membrane Protein Lab, Diamond Light Source, Harwell Science and Innovation Campus, Chilton, Oxfordshire, United Kingdom[f]; Rutherford Appleton Laboratory, Research Complex at Harwell, Didcot, Oxfordshire, United Kingdom[g]

SbmA protein has been proposed as a dimeric secondary transporter. The protein is involved in the transport of microcins B17 and J25, bleomycin, proline-rich antimicrobial peptides, antisense peptide phosphorodiamidate morpholino oligomers, and peptide nucleic acids into the *Escherichia coli* cytoplasm. The *sbmA* homologue is found in a variety of bacteria, though the physiological role of the protein is hitherto unknown. In this work, we carried out a functional and structural analysis to determine which amino acids are critical for the transport properties of SbmA. We created a set of 15 site-directed *sbmA* mutants in which single conserved amino acids were replaced by glycine residues. Our work demonstrated that strains carrying the site-directed mutants V102G, F219G, and E276G had a null phenotype for SbmA transport functions. In contrast, strains carrying the single point mutants W19G, W53G, F60G, S69G, N155G, R190, L233G, A344G, T255G, N308G, and R385G showed transport capacities indistinguishable from those of strains harboring a wild-type *sbmA*. The strain carrying the Y116G mutant exhibited mixed phenotypic characteristics. We also demonstrated that those *sbmA* mutants with severely impaired transport capacity showed a dominant negative phenotype. Electron microscopy data and *in silico* three-dimensional (3D) homology modeling support the idea that SbmA forms a homodimeric complex, closely resembling the membrane-spanning region of the ATP-binding cassette transporter family. Direct mapping of the *sbmA* single point mutants on the protein surface allowed us to explain the observed phenotypic differences in transport ability.

SbmA is an inner membrane protein that would seem to be dispensable for cell viability since no apparent growth phenotype was found in *sbmA* mutants (1, 2). A physiological role of SbmA has not been found yet; however, it is interesting that the protein is found in a large number of organisms, including plant symbionts and animal pathogens in which the homologue protein has a relevant phenotype (3–5). In the legume endosymbiont *Sinorhizobium meliloti*, the *bacA* gene encodes a 420-amino-acid protein that is 64% identical to SbmA. Furthermore, SbmA is functionally interchangeable with *S. meliloti* BacA (6). BacA is required for the development of *S. meliloti* bacteroids within plant cells (4, 7) and for the resistance to nodule-specific cysteine-rich antimicrobial peptides (NCR AMPs) produced by host plants (8). Similarly, the *Brucella abortus* BacA was shown to be essential for survival of this mammalian pathogen in macrophages (9). BacA also favors chronic infections by *B. abortus* and *Mycobacterium tuberculosis* in BALB/c mice (3). This suggests that the presence of SbmA/BacA may offer bacteria adaptive advantages to persist in different environments leading to the establishment of chronic interactions, either infectious or endosymbiotic. Nevertheless, this could be not a general rule since Ardissone et al. (10) showed that the necessity of BacA for bacteroid differentiation is restricted to specific legume-*Rhizobium* interactions.

SbmA has been shown to transport structurally diverse substrates such as microcin B17 (1), microcin J25 (11), bleomycin (12, 13), the eukaryotic proline-rich peptides Bac7 and PR-39 (2, 14), the antisense peptide phosphorodiamidate morpholino oligomers (15), and the peptide nucleic acids (PNAs) (16). Since the only SbmA substrates hitherto reported are antimicrobial peptides, it has not been possible to relate the transport ability of this protein to the bacterial physiological functions.

The substrate multiplicity of SbmA and the absence of a deep understanding of its physiological role made necessary complementary structural analyses aimed at figuring out the true nature of this protein, which has been so far elusive. Initial bioinformatic analyses of the SbmA amino acid sequence allowed classification of the protein as a transmembrane domain (TMD), part of an ABC (ATP-binding cassette) transporter that would require a yet-unidentified nucleotide binding domain (NBD) to be fully functional (5). Nevertheless, Runti et al., in the accompanying article (17), did not find any putative NBD partner in *Escherichia coli* for SbmA and showed that SbmA-mediated transport of Bac-7(1-35) requires the transmembrane electrochemical proton gradient and that it is independent of ATP hydrolysis.

In previous reports, based on the SbmA homologue BacA, it was suggested that SbmA could have 7 TM helices (4, 5). However, a study

Received 10 July 2013 Accepted 17 September 2013
Published ahead of print 27 September 2013
Address correspondence to Paula A. Vincent, pvincent@fbqf.unt.edu.ar, or Marco Scocchi, mscocchi@units.it.
N.C. and G.R. contributed equally to this work.
Supplemental material for this article may be found at http://dx.doi.org/10.1128/JB.00824-13.
Copyright © 2013, American Society for Microbiology. All Rights Reserved.
doi:10.1128/JB.00824-13

Downloaded from https://journals.asm.org/journal/jb on 24 February 2022 by 2a01:4f9:3b:1ae9::.

TABLE 1 Bacterial strains and plasmids used in this work

Strain or plasmid	Characteristics	Source or reference
Bacterial strains		
MC4100	F^- *araD139* Δ*(argF-lac)205* λ^- *rpsL150* (Sm^r) *ftbB5301 relA1 deoC1 pstF25*	CGSC[a]
MCR100	MC4100 Δ*sbmA*	41
Plasmids		
pMC01	Cm^r; pACYCDuet-1 vector with *sbmA* gene including its putative promoter region (300 bp upstream of start codon).	This study
pVC01	Km^r; pET28b(+) vector with *sbmA* gene including its putative promoter region (300 bp upstream of start codon).	This study
pW19G	*sbm*AW19G in pACYCDuet-1	This study
pW53G	*sbm*AW53G in pACYCDuet-1	This study
pF60G	*sbm*AF60G in pACYCDuet-1	This study
pS79G	*sbm*AS79G in pACYCDuet-1	This study
pV102G	*sbm*AV102G in pACYCDuet-1	This study
pY116G	*sbm*AY116G in pACYCDuet-1	This study
pN155G	*sbm*AN155G in pACYCDuet-1	This study
pR190G	*sbm*AR190G in pACYCDuet-1	This study
pF219G	*sbm*AF219G in pACYCDuet-1	This study
pL233G	*sbm*AL233G in pACYCDuet-1	This study
pT255G	*sbm*AT255G in pACYCDuet-1	This study
pE276G	*sbm*AE276G in pACYCDuet-1	This study
pN308G	*sbm*AN308G in pACYCDuet-1	This study
pA344G	*sbm*AA344G in pACYCDuet-1	This study
pR385G	*sbm*AR385G in pACYCDuet-1	This study

[a] CGSC, *E. coli* Genetic Stock Center.

in which the C terminus of *E. coli* inner transmembrane proteins was fused to green fluorescent protein (GFP) revealed that the SbmA C terminus is orientated to the cytoplasm (18). This observation is in agreement with an SbmA model having 8 TM domains. In addition, Runti et al. (17) by means of a two-hybrid assay showed that SbmA forms homodimers and provided indirect evidence that both C and N termini of SbmA are orientated to the cytoplasm.

In order to gain further insights into the nature of SbmA, we pursued a study of the transport ability of this protein and investigated the structural determinants that might play a role in this process. In this work, we show that single point mutations of the SbmA sequence lead to differential transport properties for several substrates. We also present a low-resolution molecular structure of the transporter obtained by electron microscopy and a three-dimensional (3D) *in silico* homology model. The structural information supports the hypothesis that SbmA is a dimeric protein, as reported by Runti et al. (17). Direct mapping of the *sbmA* single point mutants on the protein surface allowed us to explain the observed phenotypic differences in MccJ25, MccB17, bleomycin, Bac7(1-16), and PR-39(1-18) transport ability. Furthermore, among the SbmA mutants with null transport activity, three showed negative dominance, suggesting that these amino acids might affect the substrate transport or the protein dimerization.

MATERIALS AND METHODS

Bacterial strains and growth conditions. The *E. coli* K-12 strains and plasmids used in this work are described in Table 1. The minimal medium used was M9 minimal salts with 0.2% glucose, 1 μg ml^{-1} vitamin B_1, and 1 mM $MgSO_4$. Alternatively, Mueller-Hinton (MH) broth (Difco) was used. Solid medium contained 1.5% agar. When required, chloramphenicol or kanamycin was added at the final concentration of 30 μg ml^{-1}.

Peptides. Bac7(1-16) and the dipyrromethene boron difluoride (BODIPY) fluorescently labeled derivative Bac7(1-16)-BY have been prepared as previously described (19). PR-39(1-18) has been prepared as described previously (20). MccJ25 was purified by high-performance liquid chromatography as previously described (21). MccB17 was obtained according to the protocol described by Davagnino et al. (22). Bleomycin (Fluka) was obtained from Sigma-Aldrich.

Construction of site-directed mutants. Site-directed mutagenesis was carried out using the strategy previously described by LeVier and Walker (5). Plasmid pMC01 carrying the *E. coli sbmA* gene, with the putative promoter region 300 bp upstream from the start codon, was used as the template DNA. All codons for the targeted amino acids were changed to GGA (glycine). The derivative plasmids each harboring a different point mutated *sbmA* were transformed into competent MC4100 and MC4100 Δ*sbmA E. coli* (MCR100), and the resulting strains were named according to the mutation present in the plasmid (amino acid replaced-position-glycine).

Sensitivity test. Sensitivity to antimicrobial compounds was tested by a spot-on-lawn assay as follows. Double dilutions of different antimicrobials were spotted (10 μl) onto M9 plates and dried. Stationary-phase culture aliquots (50 μl) were mixed with 3 ml of top agar (M9 containing 0.7% agar) and overlaid onto the plates. After overnight incubation, the plates were examined for different degrees of inhibition.

The antibiotic stock solutions used in the assays were 470 μM MccJ25, 700 μM bleomycin, 312 μM Bac7(1-16), 212 μM PR-39, and 4.8 μM MccB17.

Flow cytometric analysis. Uptake of BODIPY-labeled Bac7(1-16) in *E. coli* cells was determined by flow cytometry using a Cytomics FC500 instrument (Beckman-Coulter, Inc.) equipped as previously described (14). Cultures of mid-log-phase bacteria were harvested, diluted to 10^6 CFU ml^{-1} in MH broth, incubated with 0.25 μM Bac7(1-16)-BODIPY at 37°C for 10 min, and immediately analyzed. All experiments were conducted in triplicate, and data were expressed as mean fluorescence intensity (MFI) ± standard deviation (SD). Data analysis was performed with the FCS Express V3 software (De Novo Software, CA).

Membrane extraction. Overnight cultures of the defined strains were diluted into 10 ml of fresh MH broth and grown until mid-log phase. The cells were collected by centrifugation (2,200 × *g*, 10 min, 9°C) and washed three times with 10 mM Tris-HCl, pH 8. The pellets were resuspended in 0.4 ml of 0.5 M sucrose in 10 mM Tris-HCl, pH 8. Lysozyme was added to a final concentration of 20 μg ml^{-1}, and the samples were incubated for 10 min at room temperature. After dilution of the sample 1:1 with 10 mM Tris-HCl, pH 8, EDTA was added to a final concentration of 1 mM and the samples were incubated for 10 min at room temperature. The cells were washed three times with 0.25 M sucrose in 10 mM Tris-HCl, pH 8, and then resuspended in 2 ml of 10 mM Tris-HCl, pH 8. Cells were disrupted by three cycles of freezing-thawing, and lysed cells were centrifuged at 2,000 × *g* at room temperature for 10 min. $MgSO_4$ and DNase were sequentially added to the lysed cells to the respective final concentrations of 20 mM and 0.1 mg ml^{-1}. After 30 min of incubation at 37°C, the lysates were centrifuged at 2,000 × *g* at room temperature for 10 min, and the supernatant, corresponding to the cytoplasmic fraction, was discarded. The membrane pellet was washed three times with 10 mM Tris-HCl, pH 8, and resuspended in 1% Triton X-100. After incubation at 4°C for 10 min, the total membrane extract in the supernatant was collected by centrifugation at 16,000 × *g* for 10 min. Protein concentration was determined by the bicinchoninic acid (BCA) assay (Pierce) according to the instructions of the manufacturer.

Total lysate preparation. One milliliter of mid-log-phase-grown bacteria was pelleted in a 2-ml tube by centrifugation at 8,000 × *g* for 5 min and resuspended in the appropriate volume of sample buffer (3% SDS [wt/vol], 0.1 M dithiothreitol [DTT], 7.5% glycerol [wt/vol], 0.0125% bromophenol blue in 0.125 M Tris-HCl, pH 6.8) in order to normalize the concentration of cells per ml. Bacteria were then lysed by freezing them at −20°C, sonicating them for 10 s at 35 kHz, and heating them at 80°C for 10 min.

Western blotting. After being resolved by SDS-PAGE, the proteins were transferred to a nitrocellulose membrane using a semidry transfer apparatus (Bio-Rad) at 20 V for 30 min and the membrane was stained with Ponceau Red. For the detection, the membrane was blocked over-

Downloaded from https://journals.asm.org/journal/jb on 24 February 2022 by 2a01:4f9:3b:1ae9::.

TABLE 2 Sensitivity of *E. coli* strain MCR100 carrying site-directed *sbmA* mutants

Strain	MIC (μM), comparison[a]				
	MccJ25	MccB17	Bleomycin	Bac7(1-16)	PR-39(1-18)
MC4100	0.91	0.3	5.5	39	26.5
MCR100	R	R	21.8	156	106
MCR100(pMC01)	0.455	0.15	1.4	9.75	13.25
MCR100(pW19G)	0.455 =	0.15 =	1.4 =	9.75 =	26.5 =
MCR100(pW53G)	0.455 =	0.15 =	1.4 =	19.5 =	13.25 =
MCR100(pF60G)	0.455 =	0.15 =	1.4 =	19.5 =	32 =
MCR100(pS79G)	0.455 =	0.15 =	1.4 =	19.5 =	13.25 =
MCR100(pV102G)	R X	R X	R X	156 X	106 X
MCR100(pY116G)	0.455 =	1.2 ↓	3.4 ↑	78 ↓	53 ↓
MCR100(pN155G)	0.455 =	0.15 =	1.4 =	9.75 =	26.5 =
MCR100(pR190G)	0.455 =	0.15 =	1.4 =	19.5 =	13.25 =
MCR100(pF219G)	R X	R X	5.5 ↓	156 X	106 X
MCR100(pL233G)	0.455 =	0.15 =	1.4 =	19.5 =	13.25 =
MCR100(pT255G)	0.455 =	0.15 =	1.4 =	19.5 =	26.5 =
MCR100(pE276G)	R X	R X	21.8 X	39 ↓	106 X
MCR100(pN308G)	0.455 =	0.15 =	1.4 =	19.5 =	13.25 =
MCR100(pA344G)	0.455 =	0.15 =	1.4 =	19.5 =	26.5 =
MCR100(pR385G)	0.455 =	0.15 =	1.4 =	19.5 =	26.5 =

[a] Results are given as a concentration of the last dilution which produced a clear halo. Representative results of one of three independent experiments are shown. Abbreviations and symbols: R, no inhibition observed at the highest concentration assayed (stock solution); X, the SbmA-mediated transport was abolished, and the sensitivity value was identical to that of an Δ*sbmA* strain; ↓, the strain showed a significantly decreased sensitivity compared to the strain transformed with the wild-type plasmid pMC01; =, the strain showed the same sensitivity as that of the control strain MCR100(pMC01) or the difference was no greater than 1 dilution; ↑, the strain showed a significantly increased sensitivity compared to the control.

night in 5% milk powder in TBST solution (40 mM Tris-HCl, pH 7.5, 200 mM NaCl, 0.1% [vol/vol] Tween 20) at 4°C and then incubated for 1.5 h at room temperature with the rabbit anti-SbmA antibody (17) at a titer of 1:2,000. The membrane was washed and incubated for 1 h at room temperature with the goat anti-rabbit secondary antibody conjugated to horseradish peroxidase (HRP) (GE Healthcare) at a titer of 1:2,000. The detection of HRP was performed using the ECL Plus kit (Amersham).

Bioinformatic analysis, homology modeling, and homodimer model generation. The IUPred (23) web server was used, based on the amino acid sequence of SbmA, to evaluate the occurrence of intrinsically unstructured/disordered regions.

Two web-based servers (SWISS-MODEL [24] and I-TASSER [25]) were exploited to build a 3D homology model of the full-length *E. coli* SbmA (P0AFY6 [SBMA_ECOLI]) protomer. The STRIDE program (26) was used for the assignment of the secondary structure given the atomic coordinates of the protein homology model.

The top-scored models generated were then ranked and validated by the protein model quality predictors ProQ (27) and AIDE (28).

The best model resulting from this comparison was chosen to generate the SbmA homodimeric assembly. Namely, the coordinates of the modeled SbmA protomer were structurally aligned to the two subunits of the template structure of the multidrug ABC transporter Sav1866 from *Staphylococcus aureus* in complex with AMP-PNP (Protein Data Bank [PDB] ID 2ONJ) (29) by using the PyMOL Align tool (30).

Each of the homodimeric assemblies (wild-type [wt] SbmA and the SbmA point mutants) was subjected to 4,000 steps of steepest-descent *in vacuo* energy minimization, followed by 10,000 steps of conjugate gradient *in vacuo* energy minimization using GROMACS 4.5 (31).

Analysis of the *in vacuo* energy-minimized models was carried out by visual inspection using the PyMOL molecular graphics system (30) and assessed by the Protein Interfaces, Surfaces, and Assemblies (PISA) at the European Bioinformatic Institute (32).

Electron microscopy. SbmA protein was purified in dodecyl-maltopyranoside as described in the work of Runti et al. (17). Electron microscopy and negative staining (see Fig. S2 in the supplemental material, left panel) were carried out as described before (33). The supplemental table (Table S1) gives details on the size of the data sets used and other image processing details. SbmA samples were diluted in purification buffer to about 50 μg ml^{-1} before incubation with glow-discharged copper-carbon 400-mesh/in grids (Agar Scientific) for 30 s. The excess liquid was blotted away with Whatman no. 1 filter paper, and then the grid was washed twice with distilled water. Finally, the grid was incubated with 4% uranyl acetate solution for 30 s before blotting and drying in air. Grids were inserted into a Jeol JEM-1200 transmission electron microscope operating at 100 kV, equipped with a 2 k Gatan Orius charge-coupled device (CCD) camera (15-μm pixel size). Images were processed using the EMAN1 software suite. Particles were picked using an autoboxer routine, and then the defocus was determined and the contrast transfer function was corrected (34) using the ctfit program in the EMAN suite. After correction, a high-pass filter of 1/150 $Å^{-1}$ was applied to remove low-frequency information and also a low-pass filter was applied to a cutoff resolution of 1/15 $Å^{-1}$. After reference-free class averages were generated (see Fig.S2, right panel, in the supplemental material), the angular orientations of the characteristic views were determined using a Fourier common-line routine (35) and a starting model was calculated by back-projecting the class averages (36). Iterative refinement was carried out against the starting model (10 iterations), and after this number of iterations of refinement, the Fourier shell correlation (FSC) curve between successive iterations ceased to improve. The final 3D maps were viewed using the Chimera software, and atomic coordinates and models were fitted using the Chimera fit-to-map routine (37).

RESULTS AND DISCUSSION

Selection of highly conserved amino acids of SbmA for mutation. Based on the sequence analysis, 15 highly conserved amino acids (see Fig. S1 in the supplemental material) were chosen to be mutated. In particular, amino acids W53, S79, Y116, N155, R190, F219, T255, N308, and R385 in SbmA were selected based on their position equivalency to *S. meliloti* BacA amino acids W57, S83, Y120, N159, R194, F223, T259, N312, and R389, respectively, which were previously selected for mutation and analyzed only for bleomycin transport ability (5). The E276 residue was mutated based on its relevance in SbmA-mediated transport of the truncated proline-rich peptide Bac7(1-35) (14). Finally, five additional

Downloaded from https://journals.asm.org/journal/jb on 24 February 2022 by 2a01:4f9:3b:1ae9::.

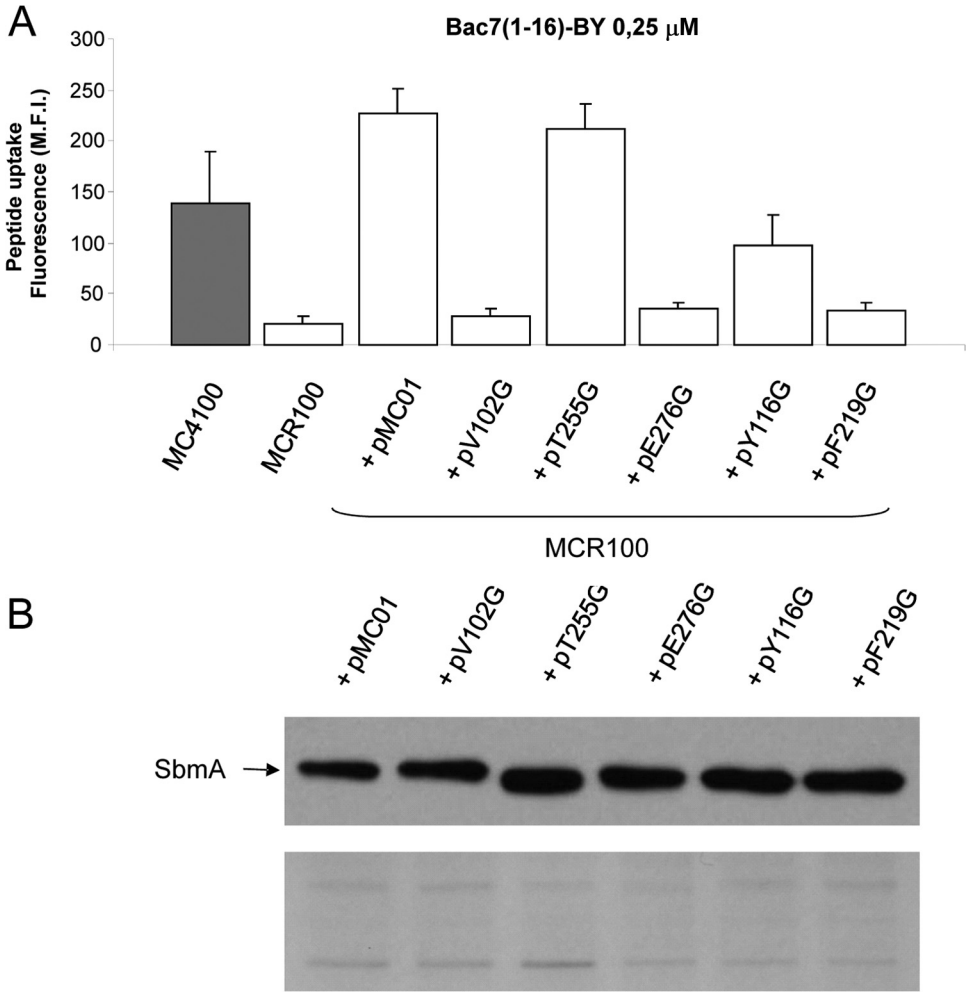

FIG 1 Transport capacity and expression of the SbmA mutants. (A) Uptake of Bac7(1-16)-BY in *E. coli* strain MCR100 carrying site-directed mutants of *sbmA* measured as MFI. Results are the means of three independent experiments with SDs. (B) Western blot analysis of the membrane protein fractions of the different mutants. Three micrograms of proteins was loaded onto the SDS-PAGE gel. Western blot analysis was performed by using a polyclonal anti-SbmA antibody. The lower panel shows Coomassie blue staining as a quantitative control. Results are representative of two independent experiments.

highly conserved amino acids in the SbmA/BacA aligned sequences (W19, F60, V102, L233, and A344) were selected to widen the analysis of point mutations to cover different regions of the protein (see Fig. S1).

In order to perform a comparative analysis of the contribution to transport activity between SbmA and its homologues, the selected conserved amino acids were replaced by glycine as previously exploited with BacA (5), although this type of substitution could likely introduce structural flexibility. Subsequently, we determined if these substitutions affected the internalization of several AMPs.

Functional study of SbmA based on mutant transport ability. Sensitivity to microcins B17 and J25, bleomycin, and PR-AMP Bac7(1-16) and PR-39 was used as an indicator of the transport ability of different point-mutated SbmAs. For all compounds tested, W19G, W53G, F60G, S79G, N155G, R190G, L233G, N308G, A344G, and R385G mutant strains had a susceptibility equivalent to that of the control strain MCR100(pMC01), which harbors a wild-type copy of *sbmA* in plasmid pMC01 (Table 2). In contrast, the V102G strain had the same behavior as the MCR100 (Δ*sbmA*) strain in showing no sensitivity to all the antibiotic peptides tested, suggesting that this mutation impairs SbmA-mediated transport. Similarly, the E276G strain was resistant to MccB17, MccJ25, bleomycin, and PR-39 and displayed a 4-fold-reduced sensitivity to Bac7(1-16) compared to that of the control (MCR100 pMC01). The F219G mutant strain also showed no sensitivity to MccJ25, MccB17, Bac7(1-16), and PR-39, although it maintained the sensitivity to bleomycin. Curiously, the Y116G mutant strain showed an increased sensitivity to bleomycin but at the same time was less sensitive to MccB17, Bac7(1-16), and PR-39 and showed no variation in susceptibility to MccJ25. Finally, the T255G strain alone had no significant reduction in sensitivity to Bac7 peptide, since only one dilution difference was observed.

The uptake of a fluorescent derivative of Bac7(1-16) linked to a BODIPY dye, Bac7(1-16)-BY, was used as direct evidence of SbmA transport activity. Figure 1A shows that the peptide uptake in V102G, E276G, and F219G mutants was dramatically reduced at a level comparable to that of the *sbmA* null mutant MCR100. As expected, complementing MCR100 with plasmid pMC01 bearing a wild-type (wt) *sbmA* increased Bac7(1-16)-BY uptake beyond the levels observed for the strain harboring a chromosomal wild-type copy of *sbmA*. The Y116G strain had a reduced Bac7(1-

Downloaded from https://journals.asm.org/journal/jb on 24 February 2022 by 2a01:4f9:3b:1ae9::.

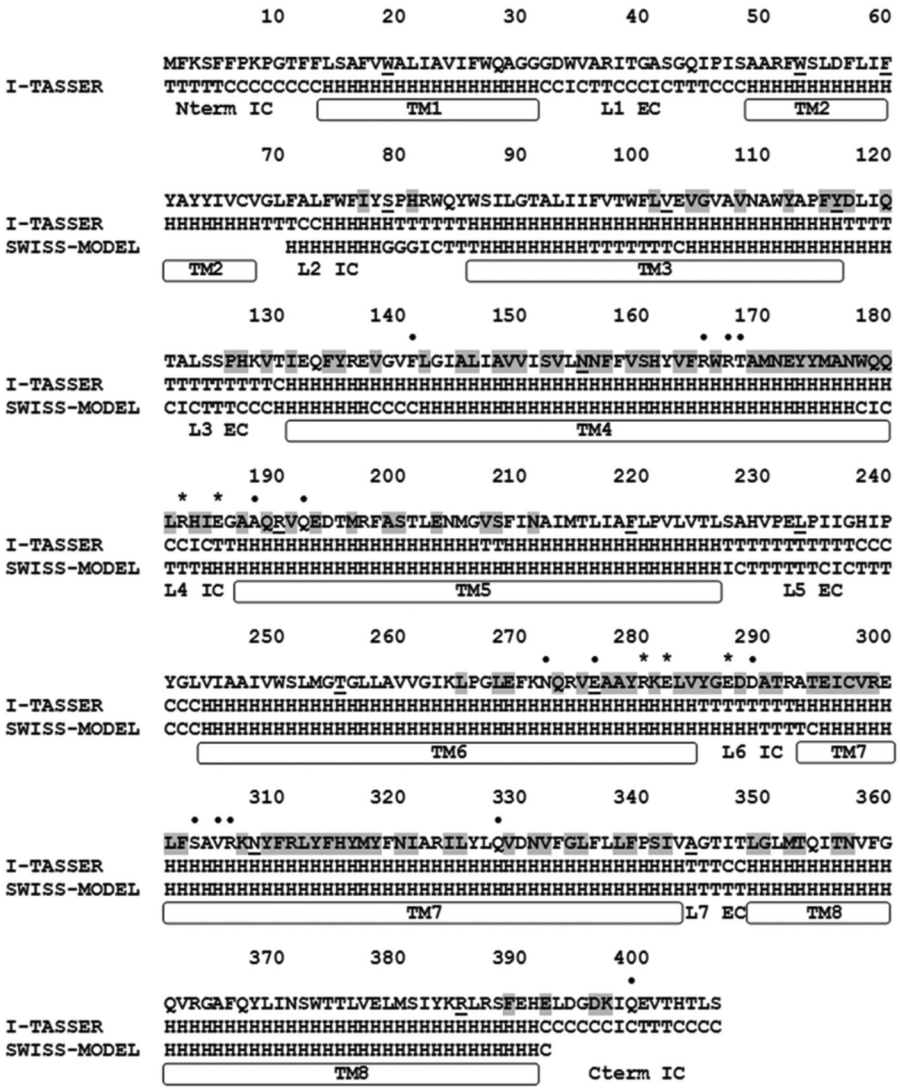

FIG 2 Secondary structure comparison of the two SbmA homology models, obtained by I-TASSER and SWISS-MODEL and extracted by STRIDE. Residues at the interface of the models of the SbmA homodimer are highlighted in gray, while black circles and stars indicate residues involved in salt bridges and in hydrogen bonds, respectively. Residues that have been selected for mutagenesis are underlined. H, alpha-helix; G, 3-helix (3/10 helix); T, hydrogen-bonded turn; TM, transmembrane helix; L, loop; IC, intracellular; EC, extracellular.

16)-BY internalization (Fig. 1A), which is in agreement with the sensitivity assay results (Table 2). While the T255G strain was slightly more resistant to Bac7(1-16), it showed no significant reduction in the Bac7(1-16)-BY uptake level (Fig. 1A). These results confirm a good correlation between the flow cytometric experiments and the MIC values.

To exclude the possibility that the reduced or null transport phenotype of V102G, E276G, and F219G strains was due to an altered expression of SbmA, Western blot analyses on both total protein lysates (data not shown) and inner membrane fractions were carried out (Fig. 1B). The results (Fig. 1B) indicate that SbmA mutants were correctly associated with the membrane fraction and that their expression levels were similar to that of the wild-type protein (encoded in the pMC01 plasmid), confirming that the phenotypes observed were a consequence of an altered SbmA functionality.

It was previously reported by Mattiuzzo et al. (14) that the SbmA E276K mutant displayed a sensitivity reduction to the eukaryotic peptides Bac7 and PR-39. In addition, LeVier and Walker (5) showed that the R284G mutation in *S. meliloti* BacA had a null phenotype for BacA-associated functions. The BacA R284 is located at a 3-amino-acid distance from the E280 residue, which is equivalent to SbmA E276. We observed that the SbmA E276G derivative has a null transport for all SbmA substrates assayed, a result that was expected considering that E276 would be located in a protein region critical for functionality. Similar phenotypes were found with the V102G and F219G substitutions. In concordance, the F223G substitution in *S. meliloti* BacA (equivalent to SbmA F219) has behavior similar to that of the *bacA* null mutant (5). Finally, the Y116G mutation (equivalent to the Y120 residue of *S. meliloti* BacA) (5) showed a dissimilar transport ability depending on the substrate used (Table 2). These observations are consistent with the differential sensitivity phenotype with respect to bleomycin and gentamicin as observed for the Y120G mutant in *S. meliloti* (5).

Downloaded from https://journals.asm.org/journal/jb on 24 February 2022 by 2a01:4f9:3b:1ae9::.

Three-dimensional homology model of SbmA. In the absence of an experimentally determined high-resolution structure of SbmA, a homology-based model may provide sufficient structural details to gain insights on its assembly and biological activity.

Prediction of the SbmA primary sequence in terms of disorder propensity (data not shown) was carried out by using the web server IUPred, which is based on pairwise energy content estimated from amino acid composition. No disordered regions, especially in terms of context-independent global disorder, were detected. Only a few carboxy-terminal residues were predicted to be flexible in terms of short, context-dependent, disordered regions.

Therefore, homology-based protein modeling was performed on the full-length amino acid sequence of *E. coli* SbmA. Two web-based servers (see Materials and Methods) produced reliable models that were further analyzed. Both models were based on proteins belonging to the ABC transporter family, whose architecture comprises two domains: a transmembrane domain (TMD) and a regulatory intracellular (IC) domain (NBD). The closer homologues of SbmA, employed as the templates by the two web-based homology modeling servers, were the TMDs of two members of the ABC transporter family. The NBD is lacking in SbmA and therefore was omitted.

The model generated by SWISS-MODEL (24) was obtained by a two-step procedure. At first, the automated mode used as the template the fitted model of the multidrug ABC transporter Sav1866 in the human cystic fibrosis transmembrane conductance regulator electron microscopy map EMD-1966 (PDB ID 4A82) (38). Then in order to improve the resulting model, the crystallographic structure of the same protein in complex with AMP-PNP (PDB ID 2ONJ) (29) was resubmitted as the template in advanced mode. The newly generated model of SbmA, encompassing residues 71 to 392, still missed the N-terminal region. Out of the four models obtained by the threading approach used by I-TASSER (25), the one ranked with the best confidence score (C-score = −1.96) was based on the coordinates of the uncharacterized ABC transporter ATP-binding protein TM_0288 (PDB ID 3QF4) (39) and comprised the full-length SbmA protein. It is interesting that the two homology models, obtained by SWISS-MODEL and I-TASSER, respectively, concur in the TM helix architecture characterized by an eight-membrane-spanning domain with both the N- and the C-terminal regions facing the intracellular (IC) space (Fig. 2). The protein model quality evaluation scores of the SWISS-MODEL and I-TASSER models, based on root mean square deviation (RMSD), TM, LG score, and MaxSub, using ProQ (27) and AIDE (28), pinpointed the best-ranked model generated by I-TASSER as the most suitable candidate to reconstruct the homodimer. Indeed, the I-TASSER model showed a predicted RMSD of 0.69 Å instead of 2.35 Å, a predicted TM score of 0.69 instead of 0.62, a predicted LG score of 4.161 instead of 2.820, and a predicted MaxSub score of 0.396 instead of 0.217 if compared to the model obtained by SWISS-MODEL.

After energy minimization, the modeled homodimer of SbmA shows a quite-extended interface involving mainly helices TM4 and TM7, with major contributions of the regions of TM5 and TM6 closer to the intracellular (IC) space and of the regions of TM3 and TM8 closer to the extracellular (EC) space. The homodimer interface buries an accessible total surface area ΔASA_{total} of 4,830.9 $Å^2$ engaging 232 residues (highlighted in gray in Fig. 2), 209 belonging to transmembrane helices, 16 to IC loops, 3 to EC

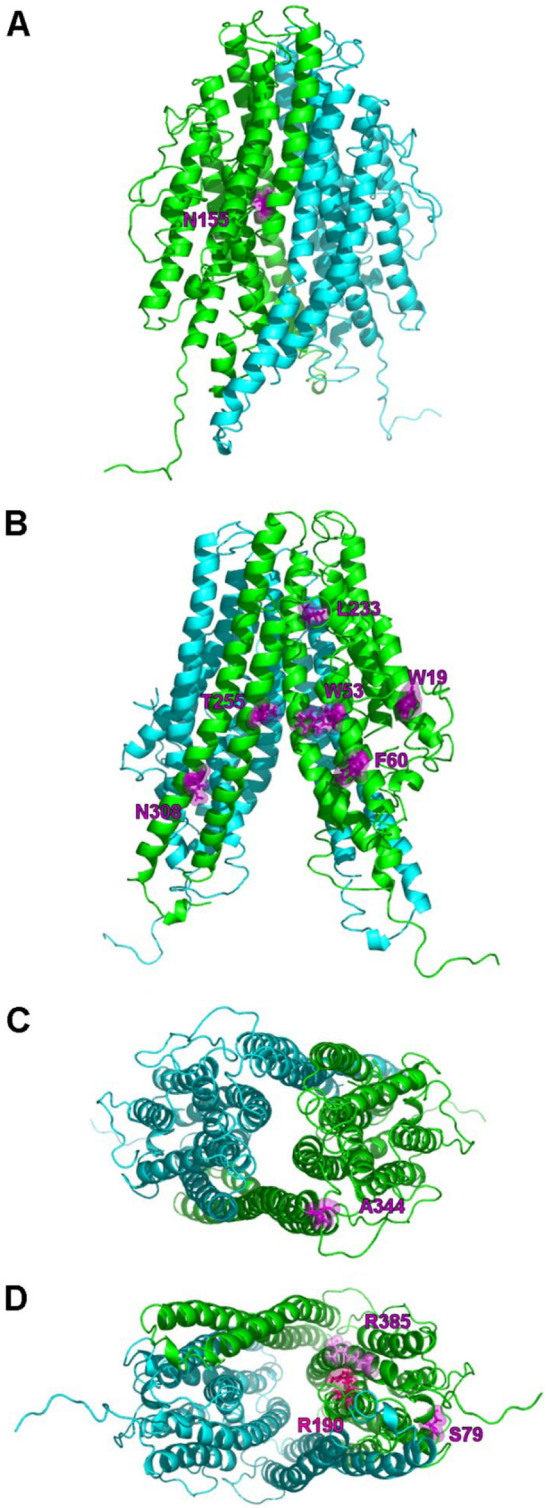

FIG 3 Mapping silent mutations on the SbmA model. Different clusters of silent mutations are depicted in purple on the model of the SbmA homodimer (the two protomers are in green and cyan, respectively). For clarity, each residue is represented only in one protomer. (A) N155 (side view); (B) W19, W53, F60, L233, T255, and N308 (side view); (C) A344 (top view from the periplasmic side of the substrate binding site); (D) S79, R190, and R385 (bottom view from the cytoplasmic side of the substrate binding site). Figures were produced by PyMOL (DeLano Scientific) (30).

Downloaded from https://journals.asm.org/journal/jb on 24 February 2022 by 2a01:4f9:3b:1ae9::.

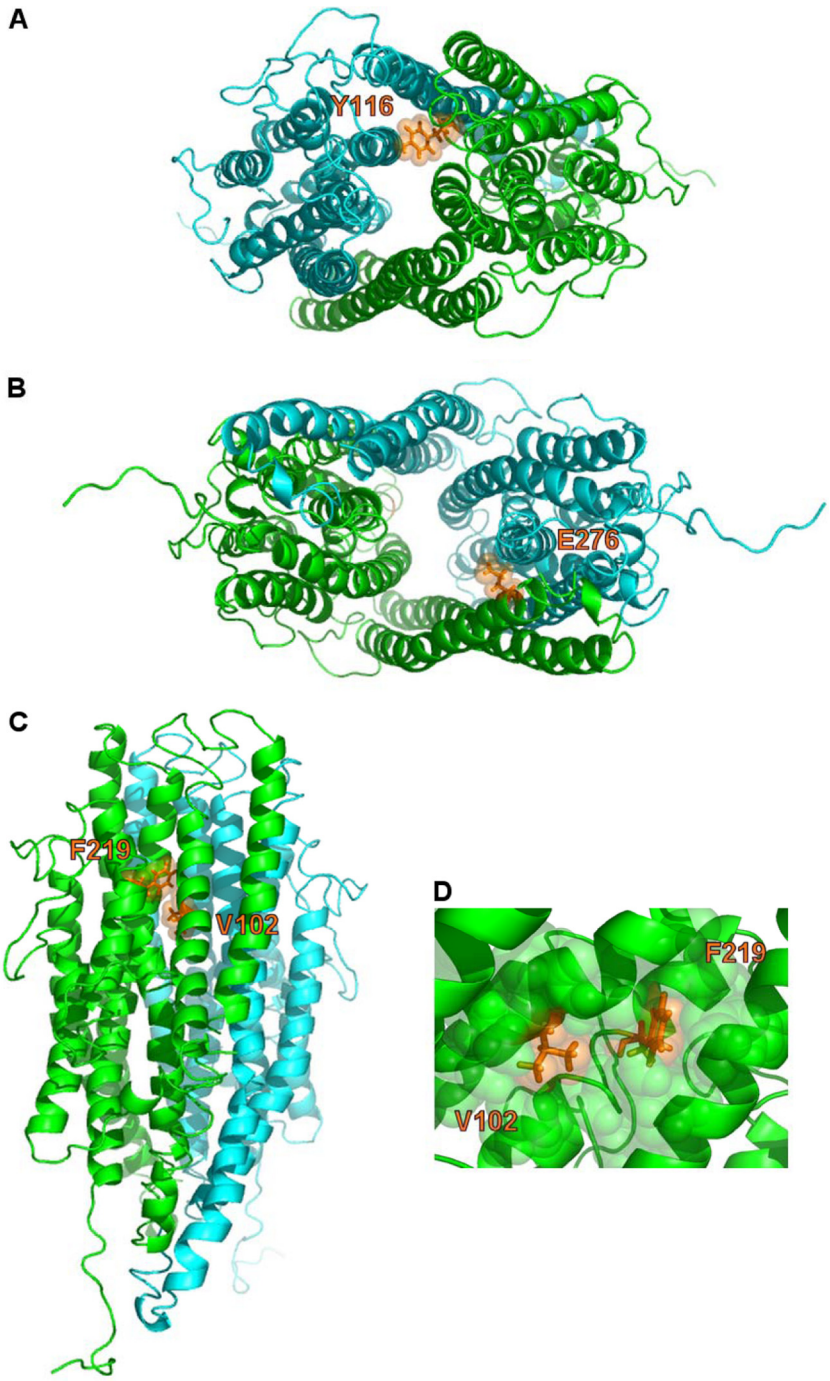

FIG 4 Mapping null mutations on the SbmA model. Different clusters of null mutations are depicted in orange on the model of the SbmA homodimer (the two protomers are in green and cyan, respectively). For clarity, each residue is represented only on one protomer. (A) Y116 (top view from the periplasmic side of the substrate binding site); (B) E276 (bottom view from the cytoplasmic side of the substrate binding site); (C and D) V102 and F219 (side view and a detail of the hydrophobic zipper, respectively). Figures were produced by PyMOL (DeLano Scientific) (30).

loops, and 4 to the C-terminal region. Among the 232 residues, 16 are engaged in a hydrogen-bonding network and 8 in the formation of 6 salt bridges (highlighted respectively by black circles and stars in Fig. 2).

The proposed model of the SbmA homodimer correctly explains the biological effects of the selected mutations (underlined in Fig. 2).

Overall, the pools of silent mutations for the transport phenotype (Table 2 and Fig. 3) do not fall in the interface of the homodimer nor are they involved in intramolecular interactions within helices of the protomer. The only exception is residue N155 (Fig. 3A), which is located at the interface between the TM3 and TM4 helices. However, these helices are loosely packed and therefore their interactions are likely to be not crucial as far as the

Downloaded from https://journals.asm.org/journal/jb on 24 February 2022 by 2a01:4f9:3b:1ae9::.

folding and/or stability of the protomer is concerned. One cluster of silent mutations (W19G, W53G, F60G, L233G, T255G, and N308G) maps on different TM helices with their side chains oriented toward the membrane (Fig. 3B). A second cluster of mutations lies on loop L5 (A344G) that is exposed to the periplasmic space (Fig. 3C), on loop L2 (S79G) on the cytoplasmic side (Fig. 3D), and on the inner (R190G) or outer (R385G) side of the transporter.

All the mutations that have an impact on the biological activity of SbmA (Table 2 and Fig. 1A), in contrast, are involved in the stability of the assembly of the homodimer (Fig. 4). In particular, a cluster of mutations (Y116G and E276G) is part of the interface between protomers (Fig. 2 and 4A and B), with E276 directly engaging in a hydrogen bond that mediates the dimer interface. Similarly, the R284G mutation in *S. meliloti* BacA, reported to be associated with a functional BacA null phenotype (5), involves a conserved residue that in SbmA model (R280) is not only part of the interface between protomers but is also engaged in a salt bridge that mediates the dimer interface.

Besides their role in the stability of the dimer, both residues (Y116G and E276G) are located in the inner side of the substrate binding cavity. Y116 may play a key role (steric hindrance) in regulating the substrate binding cavity accessibility, acting as a gate on the periplasmic compartment. This is consistent with the dissimilar transport ability observed with the Y116G mutant (Table 2) and with the differential sensitivity phenotypes in respect to bleomycin and gentamicin observed with the positional equivalent Y120G mutant in *S. meliloti* BacA (5). E276 instead is buried in the substrate binding cavity lined with aromatic residues and plays an additional key role in determining a high net negative charge that can electrostatically attract proline-rich antimicrobial peptides that are highly cationic.

A second cluster of mutations is likely to be indirectly involved in the homodimer formation. Indeed, residues V102 and F219 (Fig. 4C) are involved in the same hydrophobic zipper (Fig. 4D) that mediates not only the packing between the TM3 and TM5 helices, therefore playing a role in the protomer folding, but also their relative positions, which should result in a proper orientation of TM3 and TM5 toward the periplasm and cytoplasm, respectively, for the homodimer formation. In concordance, the *S. meliloti* BacA equivalent substitution F223G, which was predicted to be located at the end of TM5, showed no BacA-associated phenotype (5).

Structural features of SbmA transporter obtained by electron microscopy. In order to obtain structural information on the SbmA transporter and to validate our homology model, we analyzed the protein by negative-stain electron microscopy single-particle reconstruction. SbmA was purified in dodecyl maltoside (17), and after being negatively stained, it appeared homogeneous under the electron microscope. The size of the particles was around 8 nm in diameter. We have recently shown that SbmA is capable of forming dimers both *in vivo* and *in vitro* (17), and the dimensions of the particles observed were consistent with such a quaternary structure. The Coulomb density maps presented in this study were calculated with 2-fold symmetry applied throughout (Fig. 5). Initial classification of the particle set (see Fig. S2 in the supplemental material) indicated that detergent-purified SbmA forms dimers. Since the SbmA dimer is only 2 by 46 kDa, which is relatively small, even for negative-stain electron microscopy, we also used a C-terminal GFP fusion construct as a guide to

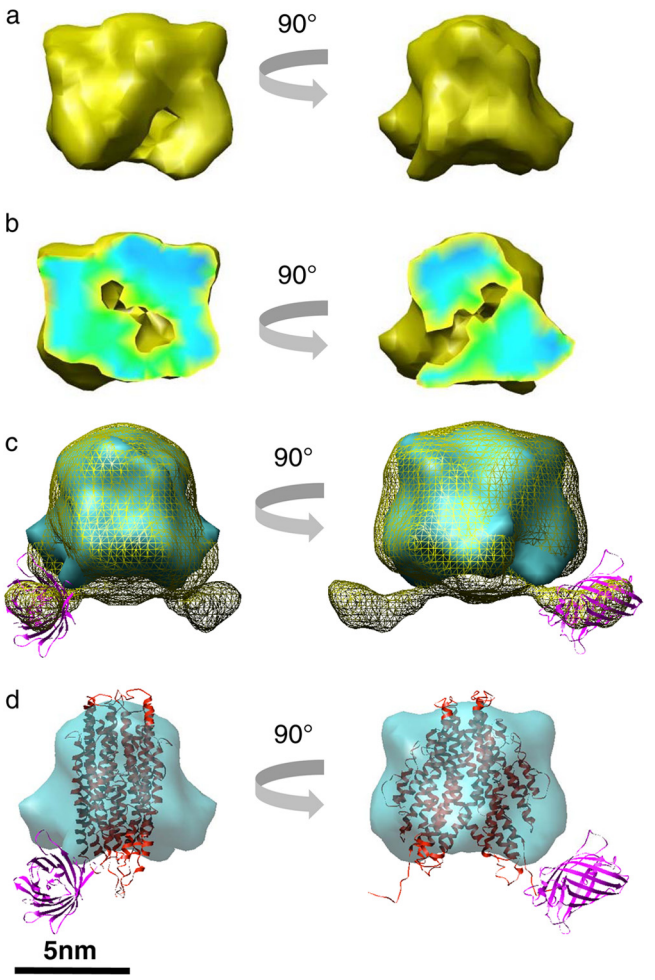

FIG 5 3D reconstructions obtained by electron microscopy of negatively stained SbmA particles. (a) Reconstruction of SbmA after removal of the GFP tag. (b) Views equivalent to panel a where the front of the structure has been sliced away to reveal internal details. (c) Structure of SbmA with GFP still attached (yellow mesh) and without it (blue surface). The purple ribbon trace shows the GFP structure fitted into the additional density. (d) The I-TASSER-derived model for the SbmA dimer has been fitted into the reconstruction lacking GFP.

locate the periplasmic and cytoplasmic portions of the particles (Fig. 5c). The resolution of the structures was calculated to be 1/19 $Å^{-1}$ for SbmA and 1/21 $Å^{-1}$ for SbmA-GFP, using a 0.5 Fourier shell correlation coefficient cutoff (see Fig. S3). The envelope portion that corresponds to SbmA is similar in the two reconstructions. The size of the SbmA dimer is 80 Å by 50 Å across and about 70 Å along the 2-fold axis, which is assumed to be perpendicular to the membrane plane (Fig. 5).

From the envelope reconstruction, the periplasmic face of the SbmA envelope appears featureless whereas the cytoplasmic face appears to be wider and with extra density on either side than the periplasmic end, suggesting that SbmA could be in an inward open or occluded state. We suspect that the protein is probably in an inward occluded state; however, at the resolution of the reconstructions we would not expect to observe any translocation pathways. The current resolution prohibits us from identifying potential domains apart from the GFP tag, which is clearly delineated by comparison with the protein after tag removal. The coordinates of

Downloaded from https://journals.asm.org/journal/jb on 24 February 2022 by 2a01:4f9:3b:1ae9::.

TABLE 3 Dominant negative character of SbmA mutants with null transport phenotype

Strain	MIC[a] (μM)				
	MccJ25	MccB17	Bleomycin	Bac7(1-16)	PR-39(1-18)
MCR100	R	R	21.8	156	106
MC4100(pVC01)	0.91	0.3	5.5	9.75	13.25
MC4100(pVC01)(pV102G)	R	R	21.8	156	106
MC4100(pVC01)(pF219G)	117.5	4.8	10.9	78	53
MC4100(pVC01)(pE276G)	R	R	21.8	156	106

[a] The table represents the sensitivity of the *E. coli* MC4100 strain cotransformed with the pVC01 plasmid (carrying the wild-type *sbmA* allele) and with either pV102G, pF219G, or pE276G. Representative results of one of several independent experiments are shown. The results are given as a concentration of the last dilution which produced a clear spot. R, no inhibition at the highest concentration assayed.

the theoretical 3D model could be fitted inside the envelope without any manipulation. The current model does not occupy all the density of the envelope, and this could be due to detergent contributions to the size of the envelope (Fig. 5b).

Dominant negative character of *sbmA* mutants with null transport activity. The production of a nonfunctional variant of a protein along with the wild-type form of it can lead to a dominant negative mutant when proteins involved form dimeric or multimeric complexes. Formation of mutant/wild-type protein complexes causes the loss of the wild-type function (40). LeVier and Walker (5) proposed that BacA might form dimers in order to be functional, since they observed that several mutant proteins, having altered phenotypes, affected the wild-type functionality of BacA when coexpressed (5). In addition, a previous report indicated that the E276K SbmA mutant exhibited negative dominance with respect to the transport of Bac7(1-35) and PR-39 (14). Considering our structural data, and since it was reported elsewhere that SbmA forms homodimers (17), we used a dominant negative assay with SbmA mutants to assess which amino acids participate in SbmA dimerization. The dominant negative character of SbmA mutants having a null phenotype regarding the transport of MccJ25, MccB17, bleomycin, Bac7(1-16), and PR-39 was evaluated.

E. coli strain MC4100 cotransformed with pVC01 plasmid (carrying the wild-type *sbmA* allele) and with either pV102G, pF219G, or pE276G was used to determine the sensitivity to the above-mentioned AMPs. All the mutants were clearly dominant (Table 3). Given that F219G, V102G, and E276G abolish or significantly reduce the substrate transport in strains having the wild-type copy of *sbmA*, we can assume that these mutants might favor the assembly of nonfunctional dimers, or even prevent dimerization. Structural data from 3D homology modeling suggest that these three amino acids might be involved in the SbmA dimerization. However, further analyses are required for a deeper understanding of amino acid participation in SbmA assembly and function.

Conclusions. In this work, we correlate structural data with functional traits of SbmA. Our observations are relevant given the elusive structural and physiological nature of this inner membrane protein. Purification of SbmA allowed electron microscopy, which along with the 3D homology model supported the dimerization evidence found by Runti et al. (17). In addition, structural evidence is consistent with SbmA having 8 TM domains with both N- and C-terminal ends facing the cytoplasm. Furthermore, we identified key amino acids in SbmA, likely involved in substrate transport or the protein dimerization. Overall, in this work we show structural and functional data that could contribute to the understanding of the cellular role that this protein plays.

ACKNOWLEDGMENTS

We thank R. Farías, F. Pomares, and R. de Cristóbal for help and useful discussions and Monica Benincasa for her help with the Bac7(1-16)-BY uptake assay. We acknowledge Richard Collins (University of Manchester, United Kingdom) and Bob Harris (University of Guelph, Canada) for electron microscopy support.

This work was funded by grants from Argentina PICT 1939 from the Agencia Nacional de Promoción Científica y Tecnológica and CIUNT 26/D439 from the Consejo de Investigaciones de la U.N.T. and by a Biotechnology and Biological Sciences Research Council grant (BBSRC: BB/H01778X/1) to K. Beis. N.C. and C.A. were recipients of a fellowship from CONICET, and P.A.V. is a Career Investigator of CONICET.

REFERENCES

1. **Lavina M, Pugsley AP, Moreno F.** 1986. Identification, mapping, cloning and characterization of a gene (*sbmA*) required for microcin B17 action on *Escherichia coli* K12. J. Gen. Microbiol. **132:**1685–1693.
2. **Pranting M, Negrea A, Rhen M, Andersson DI.** 2008. Mechanism and fitness costs of PR-39 resistance in *Salmonella enterica* serovar Typhimurium LT2. Antimicrob. Agents Chemother. **52:**2734–2741.
3. **Domenech P, Kobayashi H, LeVier K, Walker GC, Barry CE, III.** 2009. BacA, an ABC transporter involved in maintenance of chronic murine infections with *Mycobacterium tuberculosis*. J. Bacteriol. **191:**477–485.
4. **Glazebrook J, Ichige A, Walker GC.** 1993. A *Rhizobium meliloti* homolog of the *Escherichia coli* peptide-antibiotic transport protein SbmA is essential for bacteroid development. Genes Dev. **7:**1485–1497.
5. **LeVier K, Walker GC.** 2001. Genetic analysis of the *Sinorhizobium meliloti* BacA protein: differential effects of mutations on phenotypes. J. Bacteriol. **183:**6444–6453.
6. **Ichige A, Walker GC.** 1997. Genetic analysis of the *Rhizobium meliloti bacA* gene: functional interchangeability with the *Escherichia coli sbmA* gene and phenotypes of mutants. J. Bacteriol. **179:**209–216.
7. **Marlow VL, Haag AF, Kobayashi H, Fletcher V, Scocchi M, Walker GC, Ferguson GP.** 2009. Essential role for the BacA protein in the uptake of a truncated eukaryotic peptide in *Sinorhizobium meliloti*. J. Bacteriol. **191:**1519–1527.
8. **Haag AF, Baloban M, Sani M, Kerscher B, Pierre O, Farkas A, Longhi R, Boncompagni E, Herouart D, Dall'angelo S, Kondorosi E, Zanda M, Mergaert P, Ferguson GP.** 2011. Protection of *Sinorhizobium* against host cysteine-rich antimicrobial peptides is critical for symbiosis. PLoS Biol. **9:**e1001169. doi:10.1371/journal.pbio.1001169.
9. **LeVier K, Phillips RW, Grippe VK, Roop RM, II, Walker GC.** 2000. Similar requirements of a plant symbiont and a mammalian pathogen for prolonged intracellular survival. Science **287:**2492–2493.
10. **Ardissone S, Kobayashi H, Kambara K, Rummel C, Noel KD, Walker GC, Broughton WJ, Deakin WJ.** 2011. Role of BacA in lipopolysaccharide synthesis, peptide transport, and nodulation by *Rhizobium* sp. strain NGR234. J. Bacteriol. **193:**2218–2228.
11. **Salomon RA, Farias RN.** 1995. The peptide antibiotic microcin 25 is imported through the TonB pathway and the SbmA protein. J. Bacteriol. **177:**3323–3325.

Downloaded from https://journals.asm.org/journal/jb on 24 February 2022 by 2a01:4f9:3b:1ae9::.

12. **Yorgey P, Lee J, Kordel J, Vivas E, Warner P, Jebaratnam D, Kolter R.** 1994. Posttranslational modifications in microcin B17 define an additional class of DNA gyrase inhibitor. Proc. Natl. Acad. Sci. U. S. A. **91:** 4519–4523.
13. **Wehmeier S, Arnold MF, Marlow VL, Aouida M, Myka KK, Fletcher V, Benincasa M, Scocchi M, Ramotar D, Ferguson GP.** 2010. Internalization of a thiazole-modified peptide in *Sinorhizobium meliloti* occurs by BacA-dependent and -independent mechanisms. Microbiology **156:** 2702–2713.
14. **Mattiuzzo M, Bandiera A, Gennaro R, Benincasa M, Pacor S, Antcheva N, Scocchi M.** 2007. Role of the *Escherichia coli* SbmA in the antimicrobial activity of proline-rich peptides. Mol. Microbiol. **66:**151–163.
15. **Puckett SE, Reese KA, Mitev GM, Mullen V, Johnson RC, Pomraning KR, Mellbye BL, Tilley LD, Iversen PL, Freitag M, Geller BL.** 2012. Bacterial resistance to antisense peptide phosphorodiamidate morpholino oligomers. Antimicrob. Agents Chemother. **56:**6147–6153.
16. **Ghosal A, Vitali A, Stach JE, Nielsen PE.** 2013. Role of SbmA in the uptake of peptide nucleic acid (PNA)-peptide conjugates in *E. coli*. ACS Chem. Biol. **8:**360–367.
17. **Runti G, Lopez Ruiz MDC, Stoilova T, Hussain R, Jennions M, Choudhury HG, Benincasa M, Gennaro R, Beis K, Scocchi M.** 2013. Functional characterization of SbmA, a bacterial inner membrane transporter required for importing the antimicrobial peptide Bac7(1-35). J. Bacteriol. **195:**5343–5351.
18. **Daley DO, Rapp M, Granseth E, Melen K, Drew D, von Heijne G.** 2005. Global topology analysis of the *Escherichia coli* inner membrane proteome. Science **308:**1321–1323.
19. **Scocchi M, Mattiuzzo M, Benincasa M, Antcheva N, Tossi A, Gennaro R.** 2008. Investigating the mode of action of proline-rich antimicrobial peptides using a genetic approach: a tool to identify new bacterial targets amenable to the design of novel antibiotics. Methods Mol. Biol. **494:**161–176.
20. **Chan YR, Zanetti M, Gennaro R, Gallo RL.** 2001. Anti-microbial activity and cell binding are controlled by sequence determinants in the antimicrobial peptide PR-39. J. Invest. Dermatol. **116:**230–235.
21. **Blond A, Peduzzi J, Goulard C, Chiuchiolo MJ, Barthelemy M, Prigent Y, Salomon RA, Farias RN, Moreno F, Rebuffat S.** 1999. The cyclic structure of microcin J25, a 21-residue peptide antibiotic from *Escherichia coli*. Eur. J. Biochem. **259:**747–755.
22. **Davagnino J, Herrero M, Furlong D, Moreno F, Kolter R.** 1986. The DNA replication inhibitor microcin B17 is a forty-three-amino-acid protein containing sixty percent glycine. Proteins **1:**230–238.
23. **Dosztanyi Z, Csizmok V, Tompa P, Simon I.** 2005. IUPred: web server for the prediction of intrinsically unstructured regions of proteins based on estimated energy content. Bioinformatics **21:**3433–3434.
24. **Arnold K, Bordoli L, Kopp J, Schwede T.** 2006. The SWISS-MODEL workspace: a web-based environment for protein structure homology modelling. Bioinformatics **22:**195–201.
25. **Zhang Y.** 2008. I-TASSER server for protein 3D structure prediction. BMC Bioinformatics **9:**40. doi:10.1186/1471-2105-9-40.
26. **Heinig M, Frishman D.** 2004. STRIDE: a web server for secondary structure assignment from known atomic coordinates of proteins. Nucleic Acids Res. **32:**W500–W502.
27. **Wallner B, Elofsson A.** 2003. Can correct protein models be identified? Protein Sci. **12:**1073–1086.
28. **Mereghetti P, Ganadu ML, Papaleo E, Fantucci P, De Gioia L.** 2008. Validation of protein models by a neural network approach. BMC Bioinformatics **9:**66. doi:10.1186/1471-2105-9-66.
29. **Dawson RJ, Locher KP.** 2007. Structure of the multidrug ABC transporter Sav1866 from *Staphylococcus aureus* in complex with AMP-PNP. FEBS Lett. **581:**935–938.
30. **DeLano W.** 2002. The PyMOL molecular graphics system. DeLano Scientific LLC, Palo Alto, CA.
31. **Hess B, Kutzner C, van der Spoel D, Lindahl E.** 2008. GROMACS 4: algorithms for highly efficient, load-balanced, and scalable molecular simulation. J. Chem. Theory Comput. **4:**435–447.
32. **Krissinel E, Henrick K.** 2007. Inference of macromolecular assemblies from crystalline state. J. Mol. Biol. **372:**774–797.
33. **Zhang L, Aleksandrov LA, Riordan JR, Ford RC.** 2011. Domain location within the cystic fibrosis transmembrane conductance regulator protein investigated by electron microscopy and gold labelling. Biochim. Biophys. Acta **1808:**399–404.
34. **Ludtke SJ, Baldwin PR, Chiu W.** 1999. EMAN: semiautomated software for high-resolution single-particle reconstructions. J. Struct. Biol. **128:**82–97.
35. **Van Heel M.** 1987. Angular reconstitution: a posteriori assignment of projection directions for 3D reconstruction. Ultramicroscopy **21:**111–123.
36. **Orlova EV.** 2000. Structural analysis of non-crystalline macromolecules: the ribosome. Acta Crystallogr. D Biol. Crystallogr. **56:**1253–1258.
37. **Pettersen EF, Goddard TD, Huang CC, Couch GS, Greenblatt DM, Meng EC, Ferrin TE.** 2004. UCSF Chimera—a visualization system for exploratory research and analysis. J. Comput. Chem. **25:**1605–1612.
38. **Rosenberg MF, O'Ryan LP, Hughes G, Zhao Z, Aleksandrov LA, Riordan JR, Ford RC.** 2011. The cystic fibrosis transmembrane conductance regulator (CFTR): three-dimensional structure and localization of a channel gate. J. Biol. Chem. **286:**42647–42654.
39. **Hohl M, Briand C, Grutter MG, Seeger MA.** 2012. Crystal structure of a heterodimeric ABC transporter in its inward-facing conformation. Nat. Struct. Mol. Biol. **19:**395–402.
40. **Herskowitz I.** 1987. Functional inactivation of genes by dominant negative mutations. Nature **329:**219–222.
41. **Corbalan NS, Adler C, de Cristobal RE, Pomares MF, Delgado MA, Vincent PA.** 2010. The *tolC* locus affects the expression of *sbmA* through sigmaE activity increase. FEMS Microbiol. Lett. **311:**185–192.

Downloaded from https://journals.asm.org/journal/jb on 24 February 2022 by 2a01:4f9:3b:1ae9::.